PROTEINS: Structure, Function, and Genetics 40:290–298 (2000)

Comparative X-Ray Analysis of the Un-Liganded Fosfomycin-Target MurA

Susanne Eschenburg[1]* **and Ernst Schönbrunn**[2]
[1]*Max-Planck-Institute for Medical Research, Department of Biophysics, Heidelberg, Germany*
[2]*Colorado State University, Department of Biochemistry and Molecular Biology, Fort Collins, Colorado*

ABSTRACT **MurA, an essential enzyme for the synthesis of the bacterial cell wall, follows an induced-fit mechanism. Upon substrate binding, the active site forms in the interdomain cleft, involving movements of the two domains of the protein and a reorientation of the loop Pro112-Pro121. We compare two structures of un-liganded MurA from *Enterobacter cloacae*: a new orthorhombic form, solved to 1.80 Å resolution, and a monoclinic form, redetermined to 1.55 Å resolution. In the monoclinic form, the loop Pro112-Pro121 stretches into solvent, while in the new form it adopts a winded conformation, thereby reducing solvent accessibility of the critical residue Cys115. In the interdomain cleft a network of 27 common water molecules has been identified, which partially shields negative charges in the cleft and stabilizes the orientation of catalytically crucial residues. This could support substrate binding and ease domain movements. Near the hinge region an isoaspartyl residue has been recognized, which is the product of post-translational modification of the genetically encoded Asn67-Gly68. The homogenous population with L-isoaspartate in both structures suggests that the modification in *Enterobacter cloacae* MurA is not a mere aging defect but rather the result of a specific in vivo process. Proteins 2000; 40:290–298.** © **2000 Wiley-Liss, Inc.**

Key words: bacterial cell wall; induced-fit mechanism; solvent network; deamidation; isoaspartate formation

INTRODUCTION

MurA (UDPGlcNAc *enol*pyruvyltransferase, EC 2.5.1.7) catalyzes the first committed step in the synthesis of the bacterial cell wall by transferring the *enol*pyruvyl moiety of phospho*enol*pyruvate (PEP) to the 3-hydroxyl of UDP-*N*-acetylglucosamine (UDPGlcNAc).[1,2] The only other enzyme known to catalyze the transfer of the intact *enol*pyruvyl moiety of PEP to a substrate is 5-*enol*pyruvyl-shikimate-3-phosphate synthase (EPSPS, EC 2.5.1.19), an essential enzyme in the biosynthesis of aromatic amino acids in plants and microbes. Despite high structural and mechanistical similarities, EPSPS and MurA are exclusively sensitive to different inhibitors. EPSPS is the target of glyphosate (N-[phosphonomethyl]glycine), the active ingredient of the broad-spectrum herbicide Roundup®.[3] MurA is inhibited by the naturally occurring antibiotic fosfomycin [(1*R*,2*S*)-1,2-epoxypropyl phosphonic acid].[4] Fosfomycin attaches covalently and irreversibly to the thiol group of Cys115 in MurA from *Enterobacter cloacae*[5] and from *Escherichia coli*.[6]

Structural and kinetic studies revealed that the reaction catalyzed by MurA follows an *induced-fit* mechanism in which the 44 kDa enzyme undergoes large conformational changes.[7–10] MurA is a two-domain protein made up by the six-fold repetition of one folding unit consisting of a four-stranded β-sheet and two parallel helices. The two globular domains are connected by a double-stranded hinge. Upon ligand binding the domains approach each other and a ten-residue loop Pro112-Pro121 containing the catalytically essential Cys115 moves towards the interdomain cleft. In the course of the creation of the catalytic cavity this loop seems to pass through multiple conformational states.[11] In the crystal structure of un-liganded MurA from *Enterobacter cloacae*, previously determined to 2 Å resolution,[7] the loop is involved in crystal contacts.

To address the question, whether other distinct conformations of the loop exist in the open MurA form, we crystallized un-liganded MurA from *Enterobacter cloacae* in a different buffer system. The new crystal form has been analyzed crystallographically to 1.8 Å resolution and revealed a winded conformation of the loop, which drastically differs from the extended conformation in the original structure of un-liganded MurA. For detailed comparison, the X-ray model of the original crystal form has been redetermined to 1.55 Å resolution. The high-resolution data clearly proved the isomerization of Asn67 to an L-isoaspartate residue hitherto not recognized in this enzyme. Furthermore, a solvent network spanning the interdomain cleft has been identified, which is independent of the crystal packing and is likely to affect the catalytic efficiency of the enzyme. The identification of such details in the *induced-fit* mechanism of MurA could

Abbreviations: EPSP synthase, 5-*enol*pyruvyl-shikimate-3-phosphate synthase [EC 2.5.1.19]; MurA, UDPGlcNAc *enol*pyruvyltransferase [EC 2.5.1.7]; $MurA_{fosfomycin}$, crystal structure of MurA from *E. coli* complexed with fosfomycin and UDPGLcNAc, PDB entry code 1UAE; $MurA_{intermediate}$, crystal structure of MurA mutant Cys115Ala from *E. coli* with reaction intermediate analog, PDB entry code 1A2N; PEP, phospho*enol*pyruvate; PIMT, protein L-isoaspartate(D-aspartate) O-methyltransferase [EC 2.1.1.77], UDPGLcNAc, uridine diphospho-*N*-acetyl-D-glucosamine.

*Correspondence to: S. Eschenburg, Max-Planck-Institute for Medical Research, Department of Biophysics, D-69120 Heidelberg, Germany. E-mail: seschen@mpimf-heidelberg.mpg.de

Received 14 December 1999; Accepted 14 March 2000

TABLE I. Data Collection Statistics[†]

Crystal	Type 1	Type 2
Space group	C2	$P2_12_12_1$
Unit cell dimensions	a = 87.2, b = 156.3, c = 84.0, β = 91.6	a = 67.4, b = 73.7, c = 77.8
Molecules/asym. unit	2	1
V_m[a] [Å^3/dalton]	3.2	2.2
Crystal size [mm]	0.4 × 0.3 × 0.2	0.4 × 0.2 × 0.2
Wavelength [Å]	0.87	1.54
Temperature [K]	120	120
Resolution range [Å]	17.0–1.55	20.0–1.80
Last shell [Å]	1.57–1.55	1.84–1.80
Measured reflections	738470	251049
Unique reflections	155426	36451
Completeness [%]	96.0 (87.1)	99.6 (99.2)
⟨I/σ(I)⟩	24.2 (3.9)	28.4 (5.8)
R_{sym}[b] [%]	4.6 (24.6)	4.6 (22.5)

[†]Values for the highest resolution shell are given in parentheses.
[a]Matthews coefficient.
[b]$R_{sym} = \Sigma_h\Sigma_i|I_{hi} - I_h|/\Sigma_{hi}I_{hi}$ where h are unique reflection indices.

be a starting point for new strategies in the design of novel antibiotic drugs. Given the increasing number of bacterial strains resistant to fosfomycin and to other antibiotics, the search for substances that block the domain movements required for MurA activity could serve as an alternative.

MATERIALS AND METHODS

Crystallization

Recombinant MurA from *Enterobacter cloacae* was expressed and purified as described.[12] Crystals were grown in two different crystal forms (Table I). The monoclinic crystal form (type1) was crystallized using cyclohexylammonium phosphate in Na/K-phosphate buffer at pH 6.5 as reported previously.[13] The new orthorhombic crystal form (type2) was grown from 10% PEG 20000 solutions containing 0.1 M MES (pH 6.5) and 30–50 mg/ml MurA enzyme. Equilibrating the hanging droplets at a temperature of 19°C against 0.5 M MES, crystals appeared overnight and grew to full size within 1 day.

Data Collection

Type1 crystal diffraction data to 1.55 Å resolution were collected from one flash-frozen crystal using synchrotron radiation from the Swiss-Norwegian beam line BM1 at ESRF in Grenoble, France (wavelength 0.87 Å; detector: Mar300 image plate scanner; cooling device: Oxford Cryosystems). Type2 crystal diffraction data to 1.80 Å were recorded from one flash-frozen crystal using CuK_α radiation from a rotating anode X-ray generator (Rigaku RU300, operated at 90 kV/50 mA; focused by Osmic mirror optics; detector: R-Axis IV image plate scanner; cooling device: Xstream, MSC). Data reduction was performed with the HKL program package.[14] A summary of data collection statistics is given in Table I.

Refinement

Structure determinations for both crystal types are based on the 2 Å model of un-liganded MurA (pdb-entry code 1NAW)[7] stripped of all solvent molecules. Molecular replacement and subsequent refinement of the structures were performed with CNS.[15] Throughout the refinement, which followed principally the same protocol for both structures, reflections with σ(I)>0 were used, leaving 3% of the data aside for calculation of the free R value.[16] In case of crystal type1, the two molecules in the asymmetric unit were refined without imposing NCS-restraints. Several rounds of minimization, simulated annealing (2,500 K starting temperature) and restrained individual B-factor refinement were carried out, interspersed by manual corrections of the model. For all molecular graphics operations the program O[17] was employed. Solvent molecules where added to the model at chemically reasonable positions were the difference density of the F_o-F_c synthesis exceeded 3.5 σ. Phosphate ions could be discriminated from water molecules by inspection of the F_o-F_c synthesis. The oxygen atoms showed difference electron density of 5σ and higher if the phosphate ions were modeled as water molecules. Refinement statistics are summarized in Table II.

The final models of un-liganded MurA include all 419 amino acid residues per molecule. The electron density for all molecules is well defined apart from the chain termini in both crystal forms and part of the loop around C115 in monomer B of crystal type1. In the monomer B loop of type1 crystals, the main chain atoms Cα and N of 113, N of 114, Cβ of 119, Cδ, and Nε of 120, as well as the side chain of 121, do not show up in the $2F_o$-F_c map contoured at 1σ and these atoms refined to temperature factors above 50 Å^2.

All atoms have been assigned unit occupancy, except for residues with alternative side-chain conformations, the 15 phosphate ions in crystal type1, and one of the glycerol molecules in crystal type2. Occupancies of alternative locations were estimated from the electron density maps. The rms error in the atomic coordinates was estimated from a cross-validated σ_A plot[18] as 0.15 Å and 0.14 Å for type1 and type2, respectively. Both structures exhibit good stereochemistry (Table II) and conform well with standard

TABLE II. Refinement Statistics

Crystal	Type 1	Type 2
Resolution range [Å]	17.0–1.55	20.0–1.80
Number of reflections used in refinement	150740	35357
Number of reflections used for R_{free}	4686	1094
R_{cryst} [%][a]	18.5	16.7
R_{free} [%][b]	20.7	19.2
Protein atoms (non-hydrogen)	6286	3143
Alternate atom positions	203	69
Water molecules	923	534
Phosphate ions	15	1
Cyclohexylammonium ions	5	0
Glycerol molecules	0	4
Mean B-factor (protein) [Å^2]	25.3	16.9
Mean B-factor (water) [Å^2]	41.7	30.0
Rmsd bond lengths [Å][c]	0.010	0.008
Rmsd bond angles [°][c]	1.8	1.5
Rmsd dihedral angles [°][c]	24.5	24.6
Rmsd improper angles [°][c]	1.26	3.48

[a]$R_{cryst} = \Sigma|F_{obs} - F_{model}|/\Sigma F_{obs}$ where F_{obs} and F_{model} are observed and calculated structure factor amplitudes, respectively.
[b]R-factor calculated for 3% randomly chosen reflections which were excluded from the refinement.
[c]rmsd: root mean square deviations from ideal values.

geometry: 94.0% (type1) and 93.3% (type2) of all non-glycine and non-proline residues have main-chain torsion angles in the most favorable region of the Ramachandran plot.[19,20] Only one residue, Ser 349, lies in a generously allowed region in crystal structures type1 and type2; none of the Φ/Ψ combinations is disallowed. Residue 67, which appears to exhibit disallowed dihedral angles, is an isoaspartate (see below), which is not correctly handled by common validation programs.

In the following all comparisons of type1 with type2 refer to molecule A of type1. Labeling of the secondary structure elements and subunits adheres to the nomenclature given previously.[7] Numbering of solvent molecules is according to crystal structure type2.

RESULTS AND DISCUSSION

Conformation of the Loop Around Cys115

The general fold of un-liganded MurA type2 follows principally that of the type1 structure (Fig. 1), which has been described in detail.[7] Superimposing the α-carbon chain of type2 on that of monomer A of type1, the average (not rms) deviation of all 419 structurally equivalent Cα atoms is 0.54 Å. While most of the protein fold and especially the orientation of the two domains relative to each other are unaltered by the crystallization conditions, three loop regions differ significantly (Fig. 1). Main chain atoms of these loops are involved in hydrogen bonding to symmetry equivalent molecules, resulting in a deviation of 4.5 Å and 2.1 Å in the Cα positions of Glu140 and Glu329, respectively. The most drastic discrepancy lies in the conformation of the catalytically important loop Pro112-Gly-Gly-Cys-Ala-Ile-Gly-Ala-Arg-Pro121 with a maximum deviation of 10.7 Å in the Cα positions of Pro121.

In type1, this loop is extended in a wide open conformation almost parallel to the upper edge of the cleft (Fig. 1). The loop position is anchored via a solvent network spanned by the charged residues Asp123 and Glu140 (Fig. 2A), which connects the tip of the loop with the first turn of the helix 123–131 (α1 of subunit IIc) as well as with the α-turn 139–142 between strands β3 and β4 of the same subunit. On the base of the loop, a β-turn is formed in residues 120–123, positioning the side chain of Val122 for hydrophobic interaction with Leu111. Thus the strictly conserved residues Leu111 and Val122 act as a spacer to separate the two sides of the loop. Apart from these intra-molecular connections, in type1 the loop is involved in interactions with neighboring molecules in the crystal. Residues 115 and 117 of molecule A mimic a short irregular β-strand with residues 157 and 159 of a symmetry-related molecule B, bulged at residues 116 and 158, respectively. The inverse interaction of residues 157 and 159 of molecule A with residues 115 and 117 of the same symmetry-related molecule B exists as well, and elongates the strand β1 of subunit IIa. In addition to these main-chain/main-chain connections, two more polar interactions including one salt-bridge, as well as two hydrophobic interactions originated by the side chain of the strictly conserved Ile117 link the loop of molecule A to the symmetry-related molecule B.

In type2 the loop is less influenced by crystal packing, with only Gly114 and two residues at the C-terminal end of the loop involved in symmetry contacts (Fig. 2B). Here the loop adopts a very different conformation, arranged in three β-turns 112–115, 116–119, and 120–123 (Fig. 2B). The last β-turn 120–123, which in type1 starts the hydrogen-bonding pattern of helix a1 at the carbonyl oxygen of Val122, is substantially displaced in the type2 structure. By a shift of almost 180° in the Ψ angle of Asp123, Val122 is dislocated by 10 Å compared to the type1 structure. The hydrogen-bond Val122 O—Ile126 N of type1 is replaced by

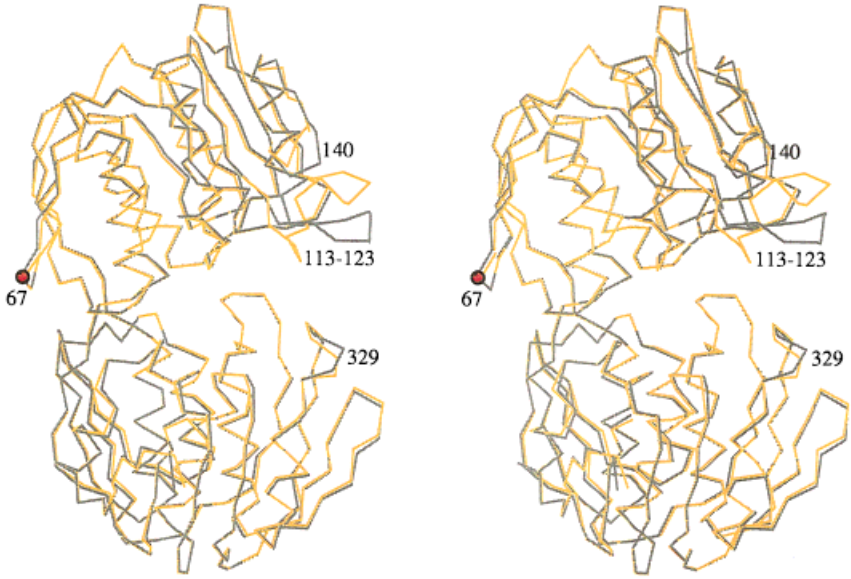

Fig. 1. Stereo representation of the optimally superimposed α-carbon chains of structures type1(gray) and type2 (orange). Ranges with significant positional deviations are labeled by residue numbers. The L-isoaspartyl residue in position 67 is designated by a red circle. Figures 1, 3, and 5 were drawn using MolScript.[34]

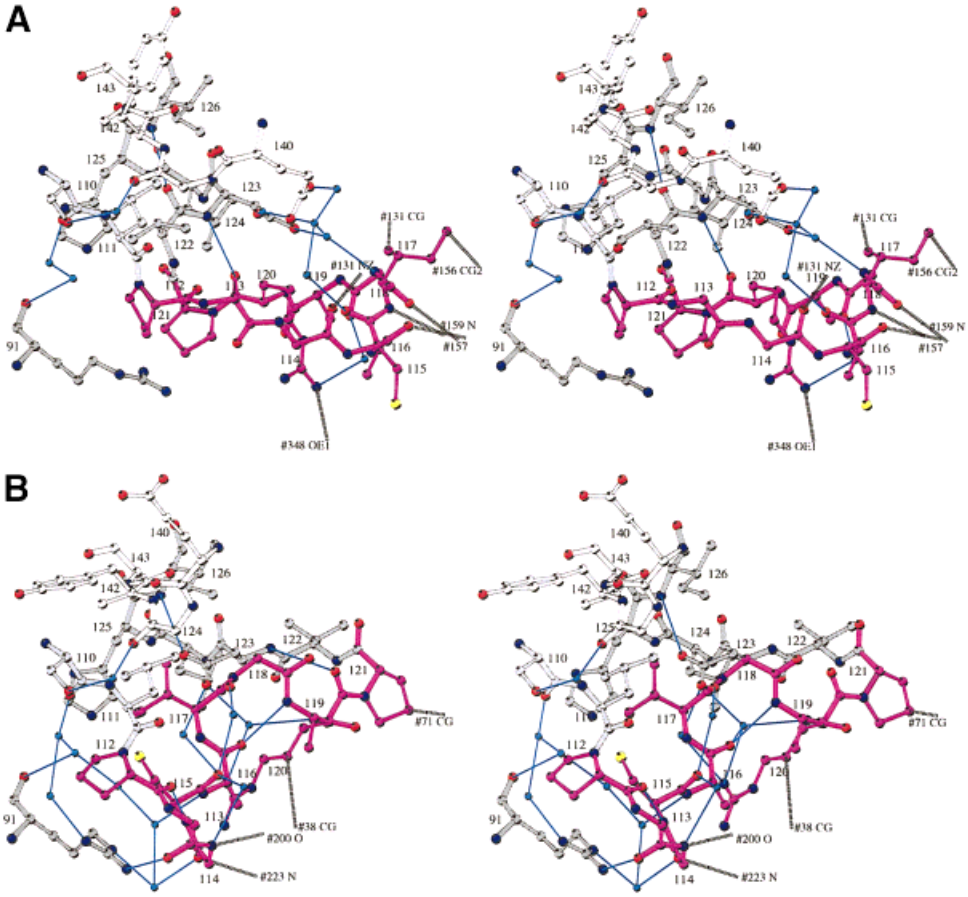

Fig. 2. Different conformations of the loop Pro112-Gly-Gly-Cys-Ala-Ile-Gly-Ala-Arg-Pro121 in un-liganded MurA. **A:** (upper stereo pair) Conformation in crystal structure type1. **B:** (lower stereo pair) Conformation in crystal structure type2. The loop itself is highlighted in magenta and the surrounding protein is shown in gray; nitrogen atoms are marked blue and oxygen red. Turquoise spheres and lines designate water molecules and hydrogen bonds, respectively. Interactions with a symmetry-related molecule are indicated by black dotted lines and the residue number of the symmetry-related residue involved. The view corresponds to the orientation of the molecule shown in Figure 1.

the side-chain interaction Asp123 OD1—Ile126 N in type2. Asp123 OD2 is hydrogen-bonded via two solvent molecules to main and side chain atoms of Arg119. A second hydrogen-bond network, which involves the strictly conserved Arg91, stabilizes the N-terminal part of the loop. A total of six solvent molecules connect Arg91 with the hydroxyl group of Ser110 and with main-chain atoms of Gly113, Gly114, and Ala116. In the type1 structure the guanidinium group Arg91 is unpaired and highly flexible with temperature factors of 50 Å^2 at its guanidinium group. The two-water chain connecting the carbonyl oxygen of Arg91 with the carbonyl oxygen of Ser110, as well as one solvent molecule

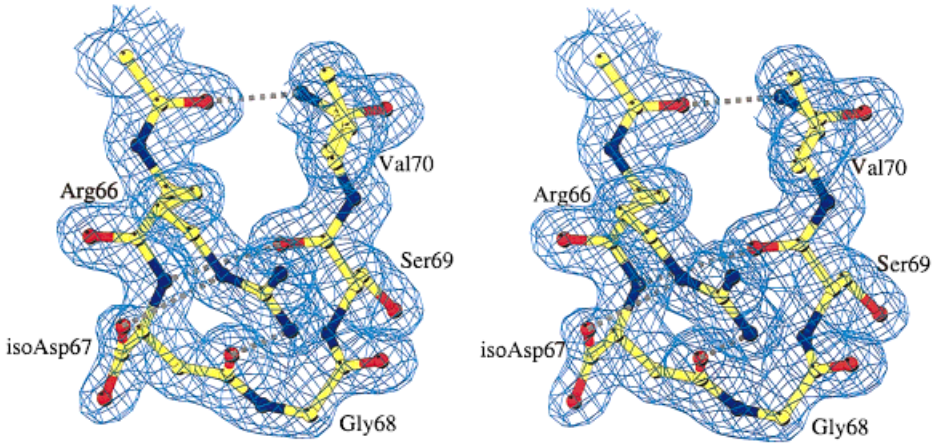

Figure 3.

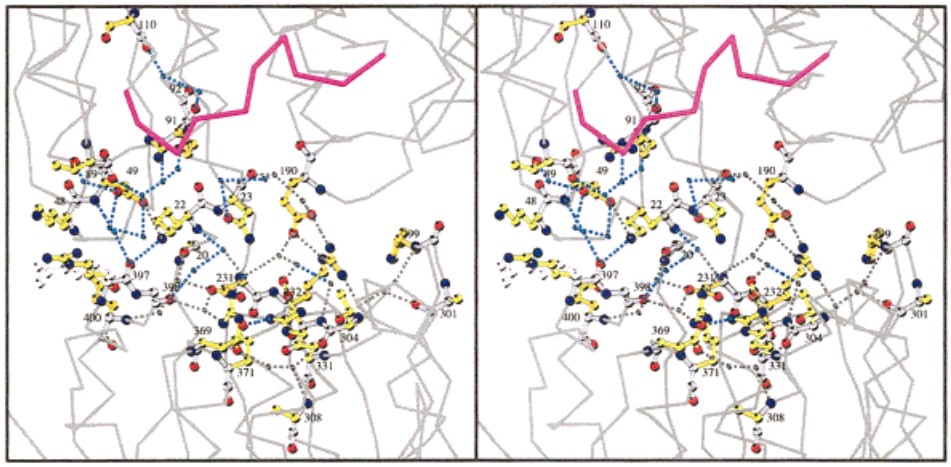

Figure 4.

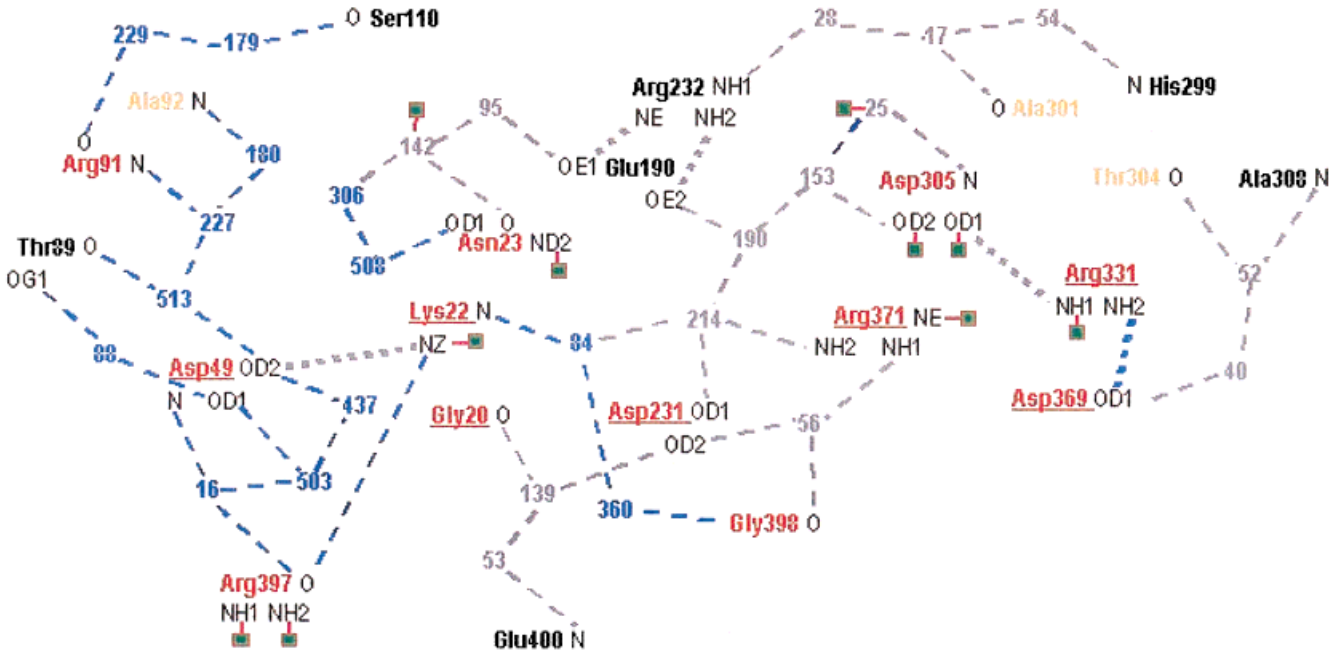

Figure 5.

that bridges the side chain of Ser110 with the carbonyl oxygen of Gly141, are conserved between type1 and type2. The side chain of the catalytic key residue Cys115, which is extremely solvent accessible in type1, folds into a partly hydrophobic cavity in type2. The cavity is formed by residues 91, 111–117, and the water network attached to Arg91. Apart from the water network, the cavity is wide open towards the enzyme's cleft. On the top of the cavity, the strictly conserved Ile117 is in hydrophobic contact with Leu111. This shielding reduces the solvent accessibility of Cys115 from 138 Å^2 in type1 to 30 Å^2 in type2, as evaluated by the program DSSP.[21]

Superimposing the main chain atoms of the loop residues 112–121 of the un-liganded forms and those of the liganded structures $MurA_{fosfomycin}$ and $MurA_{intermediate}$, the extended conformation in type1 resembles the loop in the binding state.[11] Obviously, the winded loop of type2 has to unwind upon UDPGlcNAc-binding. As described here, this transition can occur even in the absence of UDPGlcNAc: a change of ionic strength or packing forces are sufficient to unwind the loop. It has been suggested that the thiol group of Cys115 has to be activated in the course of the large movement to allow an immediate interaction of fosfomycin with Cys115.[11] Given the spatial proximity of Arg91 to Cys115 in the type2 structure, the guanidinium group of Arg91 could possibly assist in deprotonating the thiol group of the cysteine at some stage of the conformational changes.

Isoaspartate Formation

In the MurA structures type1 and type2 an unusually narrow turn is formed by residues 67–69 linking the anti-parallel strands β3 and β4 of subunit IIb at the back of the interdomain cleft (Fig. 1). The electron density could not be fit by the genetically encoded sequence Asn67-Gly68-Ser69 and clearly revealed the existence of an isoaspartyl residue in position 67 rather than asparagine (Fig. 3). Isoaspartate formation is known to occur over time in purified proteins as a post-translational aging defect through a nonenzymatic intramolecular mechanism.[22–25] The major pathway proceeds through deamidation of the asparagine side chain upon formation of a succinimidyl ring. Subsequent hydrolyzation of the succinimide at the β-carbonyl group leaves an α-carboxyl group as side chain and an extra CH_2 in the polypeptide backbone.[26]

In crystals of type2 as well as in both monomers of type1 the isoaspartate is in L-configuration with temperature factors in the range of those of the adjacent polypeptide chain. The relative low temperature factors and the excellent quality of the electron density at residue 67 reflect a homogeneous population of modified MurA molecules in the crystals, rather than a mixture of Asn, D-Asp, L-Asp, and isoAsp as suggested so far.[27] Since purification (3 days, 4°C, pH 8.0) and crystallization (2 days for type1, 1 day for type2, 19°C, pH 6.5) of *Enterobacter cloacae* MurA proceed rapidly, it is unlikely that the homogeneous modification of Asn67 to L-isoaspartate is a result of in vitro aging. Although Asn-Gly sequences as in residues 67–68 of *Enterobacter cloacae* MurA are generally most favorable for spontaneous deamidation,[26,28] isoaspartate formation appears here as a specific, possibly autocatalytic process in vivo.[29] Arg66 or Lys46, which are close to residue 67 in the three dimensional structure, could serve as general-base catalysts in the modification of Asn67.

Comparing the sequences of MurAs deposited so far 30, in 6 out of 11 organisms Asn-Gly (*E.cloacae*, *E.coli*, *Bacillus subtilis*), Asp-Gly (*Mycobacterium tuberculosis*, *Synechocystis sp*), or Glu-Gly (*Borrelia burgdorferi*, *Acinetobacter calcoaceticus*) motifs are found in sequence positions equivalent to the L-isoaspartyl site of *Enterobacter cloacae* MurA. Notably, the crystal structures of the highly homologous *E. coli* enzyme ($MurA_{fosfomycin}$ and $MurA_{intermediate}$) suggest that the *E. coli* MurA Asn67 could also be isoaspartate. The stereochemistry, implied by the deposited coordinates of the $MurA_{intermediate}$, is severely violated at Asn67 with disallowed Φ/Ψ angles and a chiral volume close to zero for the α-carbon atom. In $MurA_{fosfomycin}$ the three-membered turn 67–69 is too tight, as reflected by a hydrogen bond distance of only 2.39 Å between Asn67 N and Ser69 O.

With isoaspartate in position 67 and its extra CH_2 in the protein backbone only three residues are sufficient to tightly bend the main chain in an energetically favorable manner. One of the carboxyl oxygen atoms of the isoaspartyl side chain forms a hydrogen bond to the guanidinium group of Arg66, which is linking the three-membered turn with the carbonyl oxygens of Val44 and Pro45. The resulting compact arrangement of the solvent exposed turn might reduce the susceptibility to proteolytic degradation.

However, on the basis of the crystal structures alone, it cannot be ascertained whether the isoaspartate formation

Fig. 3. Stereo representation of the 2Fo-Fc fourier synthesis around the L-isoaspartate in position 67 in crystal type1. The electron density is contoured at 1σ. Gray dashed lines represent hydrogen bonds. The figure was drawn with BobScript.[35]

Fig. 4. Hydrogen-bonded network in the interdomain cleft of MurA (stereo representation). Residues involved in the network are shown as ball-and-stick, with side chains colored yellow, main chain in gray; nitrogen and oxygen atoms are marked blue and red, respectively. The alternative conformation of Arg397 is marked by dashed contours. Hydrogen bonds are indicated by dashed lines, solvent molecules by small dots. Gray dotted lines represent interactions, which are conserved upon ligand binding and the associated movement of the enzyme; blue dotted lines represent interactions, which are only present in the open conformation of MurA. The surrounding protein is shown as Cα trace with the loop region highlighted magenta. The coordinates are taken from structure type2. The view is frontal into the cleft and towards the hinge region.

Fig. 5. Schematic representation of the hydrogen-bonded network in the cleft of MurA. Water molecules are numbered according to structure type2. Gray lines and numbers indicate interactions and solvent molecules, respectively, which are conserved in un-liganded (structures type1 and type2) and liganded ($MurA_{fosfomycin}$ and $MurA_{intermediate}$) MurA; blue stands for interactions and solvent molecules only present in the un-liganded forms. Salt bridges are shown as bold dotted lines. Amino acids are labeled with residue names and residue numbers and color coded according to their variability in the sequences of 11 and 20 sequences of MurAs and EPSPSs, respectively: red and underlined, absolutely conserved in MurA and EPSPS; red, 100% conserved in MurA; orange, at least 90% conserved in MurA; black, less than 90% conserved in MurA. Atoms known to be involved in substrate binding are marked by green squares.

plays a functionally important role in *Enterobacter cloacae* MurA and in homologues from other organisms. The widespread existence of an enzyme with specificity for methylation of L-isoaspartyl residues in proteins [protein L-isoaspartate(D-aspartate) O-methyltransferase = PIMT],[31] which also occurs in *E. coli*[32] and presumably in *Enterobacter cloacae* as well, could hint to some regulatory mechanism involving the highly accessible isoAsp site. A mere repair function of a PIMT induced methylation[31] would not be sensible physiologically, when the nascent protein appears to be fast and uniformly modified to L-isoaspartyl protein as in the case of *Enterobacter cloacae* MurA.

Phosphate Binding Sites

In the type1 structure, which has been crystallized from high molar phosphate buffer,[13] a total of 15 phosphate ions are bound to the two protein molecules in the asymmetric unit. The phosphate ions are coordinated by solvent molecules and charged residues at the surface. The ions are distributed asymmetrically over molecules A and B in type1 crystals, except for 2 phosphate ions coordinated in both monomers by Ser162 OG, Val163 N, and Gly164 N at the N-terminus of helix α2 of subunit IIa. The coordination at this site differs in number and location of the assisting solvent molecules and is, like the other phosphate binding sites, only partially occupied. This indicates that no specific phosphate binding site exists in the open conformation of MurA. Thus, since inorganic phosphate is a product of the enzyme's reaction, the reverse reaction presumably requires the presence of *enol*pyruvyl-UDPGlcNAc to induce a conformational change allowing inorganic phosphate to bind.

Conserved Water Network in the Cleft

In un-liganded MurA an elaborate hydrogen-bonding network has been identified, which spans the open interdomain cleft (Fig. 4). The network comprises 27 water molecules mainly linking conserved residues with each other (Fig 5). Since these solvent molecules and their interactions are conserved in all three copies of un-liganded MurA, i.e., the independently refined molecules A and B of crystal type1 as well as the single molecule of crystal type2, the network is not influenced by crystal packing. While part of the water network is also present in both liganded forms, $MurA_{fosfomycin}$ and $MurA_{intermediate}$, 13 solvent molecules appear to be expelled upon substrate binding and the associated domain movements (Fig. 5).

Comparing the structures of un-liganded MurA with the liganded forms, the largest shifts in the network occur in residues Lys22, Asn23, Asp49, Thr89, and Arg397. The side chain of Arg397 is parallel to the side chain of Lys48 and thereby helps to maintain the open conformation.[7] It exhibits two alternative side chain conformations in all three copies of the un-liganded enzyme. The double conformational state is presumably due to the repulsive forces between its guanidinium group and the ε-amino group of Lys48. Upon ligand binding Arg397 swings around towards the center of the cleft to interact with fosfomycin in $MurA_{fosfomycin}$ or fluoro-PEP in $MurA_{intermediate}$. In the course of the downward movement of the upper domain, the main chain around Asp49 and Thr89-Ala92 is shifted by up to 2.7 Å, thus expelling the bound water molecules. The side chain of Asp49 takes the position formerly occupied by W503 and W437. In their new positions, the side chains of Asp49 and Arg397, as well as those of Asp49 and Lys22 form salt bridges. Lys22 and Asn23, both known to coordinate substrate/inhibitor[9,10] move towards the positionally invariant Asp231, Asp305, Arg371, and Arg331. Water molecules W95 and W142 seem to follow the moving Asn23. W142 is then in hydrogen bonding distance to the sugar nucleotide, which in turn strikes out W306 and W508. Water molecules W84 and W360 are pushed out by the movement of Lys22. The main chain nitrogen atom of Lys22 then occupies the former position of W84 and is hydrogen bonded to W214.

The water network presumably helps to arrange the extended side chains of charged residues in the cleft to ensure proper functioning of the enzyme in terms of substrate binding and associated domain movements. The 14 solvent molecules which are preserved upon substrate binding stabilize the shape of part of the UDP-GlcNAc binding moiety. They are tightly bound to the protein, reflected in a mean temperature factor of only 18.1 $Å^2$ for the type2 structure. The removable fraction of the water network mainly establishes hydrogen bonded chains between the upper and lower domain, thereby stabilizing the open conformation of the enzyme. Furthermore, some of these more loosely bound solvent molecules (mean B-factor 30.6 $Å^2$ in type2) seem to act as place holders for moving protein regions and two oxygen atoms of the sugar nucleotide.

Looking at the electrostatic potential calculated by the program GRASP 33 at the surface of the enzyme (Fig. 6), it appears that the cleft solvent partially shields negative charges in the interdomain region of the un-liganded protein, thus facilitating the approach of the negatively charged substrates.

CONCLUSIONS

The L-isoAsp consistently found in our structures of *Enterobacter cloacae* MurA are unlikely to be the result of an aging process. Given the homogeneous modification of Asn67 to L-isoAsp in three independently refined copies, isoAsp might play a functional role in *Enterobacter cloacae* MurA. Whether this interesting post-translational modification is only pressured by stereochemical necessity or whether the isoAsp site is of regulatory importance cannot be concluded from the crystal structure alone. Biochemical studies and specifically designed mutant experiments on MurA from *E. cloacae* or *E. coli* should help to better understand the physiological effects of deamidation and isoaspartate formation.

The elaborate solvent network, which spans the interdomain cleft and extends up to the catalytically important loop, might be critical for the *induced-fit* mechanism of MurA. The disruption of the cleft and loop networks presumably results in a collapse of the open state of the

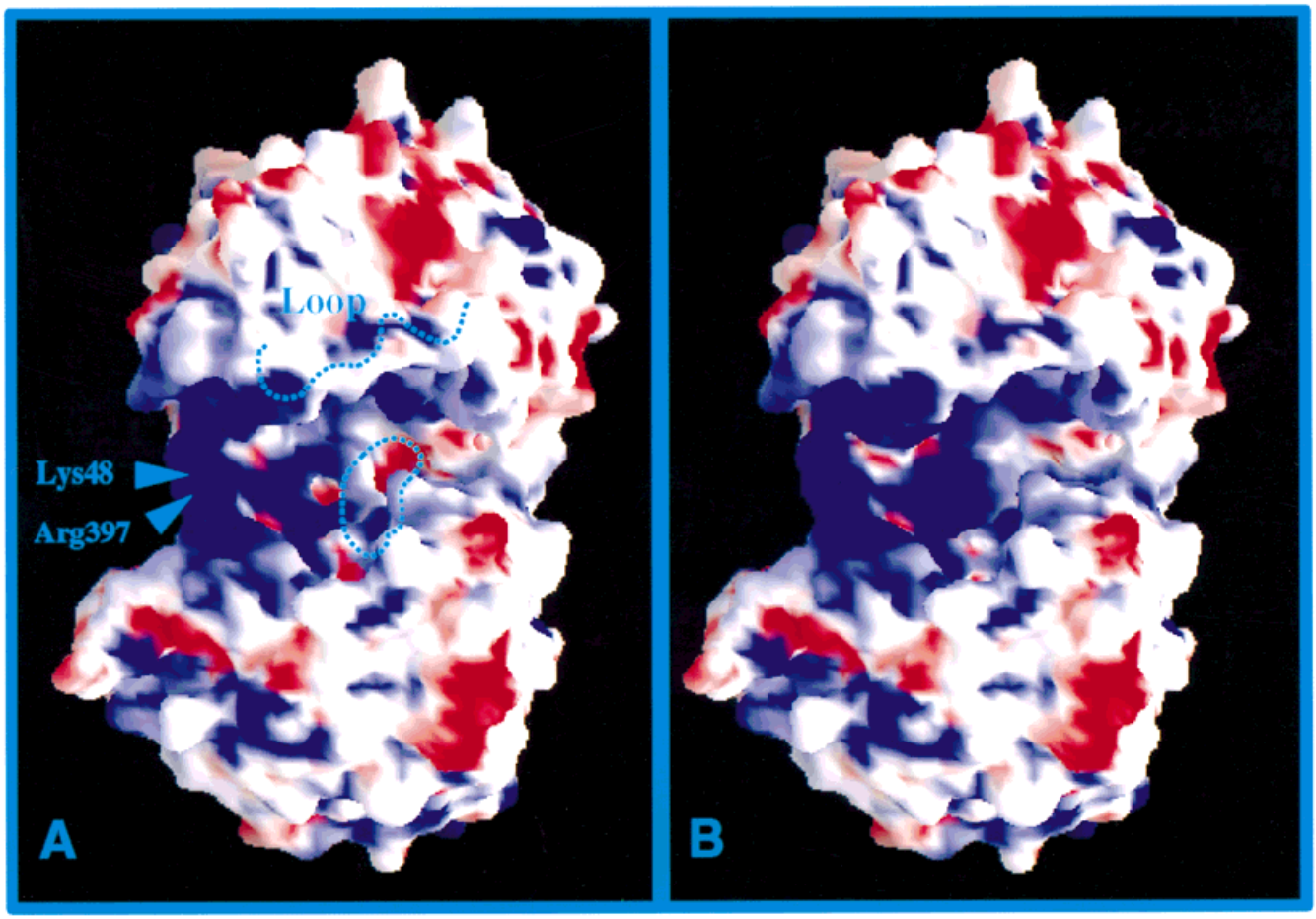

Fig. 6. Qualitative representation of the electrostatic potential on the molecular surface of un-liganded MurA (type2). **A:** Protein atoms only. **B:** Protein atoms and 27 cleft water molecules. Positive potential is indicated blue, negative potential red. Dashed lines mark the position of the ten-membered loop around Cys115 in the upper domain and of the positionally invariant Asp305, Arg331, Arg371 involved in substrate binding in the bottom domain. The molecule is in the same orientation as in Figure 5. The figure was drawn using GRASP.[33]

enzyme. The displacement of water molecules upon ligand-binding may be considered a rapid process, whereas the re-formation of a solvent network is likely to proceed slower. This is corroborated by kinetic studies on the enzyme's conformational changes, in which the transition of the open to the closed state proceeds rapidly upon substrate binding to wild-type enzyme[8,11] but is rate-limited in the opposite direction (Schönbrunn, unpublished data). These findings, and the lack of a specific phosphate binding site in the open state indicate that catalysis might proceed without a repeating conformational cycle, i.e., in the closed state only. The open conformation might represent a resting state of the enzyme, established as a result of substrate depletion. The loop conformation in type2 is more likely to reflect such a resting state than the loop in type1. As a consequence of the winded loop conformation in type2, the catalytically important Cys115 is nested in a partially hydrophobic cavity, protecting the reactive group against oxidation. The energy barrier for unwinding the coiled loop to a form required for catalysis, appears to be low, since alteration of the crystallization conditions is sufficient to stretch the loop.

ACKNOWLEDGMENTS

We thank N. Amrhein, K. Piontek and W. Blodig (ETH Zurich, Switzerland), W. Kabsch (MPI for Med. Research, Heidelberg, Germany), and K. Luger (CSU, Ft. Collins, CO) for critical discussions and help at various stages of the project.

REFERENCES

1. van Heijenoort J. Biosynthesis of the bacterial peptidoglycan unit. In: Ghuysen JM, Hakenbeck R, editors. Bacterial cell wall. Amsterdam: Elsevier; 1994. p 39–54.
2. Walsh CT, Benson TE, Kim DH., Lees WJ. The versatility of phosphoenolpyruvate and its vinyl ether products in biosynthesis. Chem Biol 1996;3:83–91.
3. Steinrücken HC, Amrhein N. The herbicide glyphosate is a potent inhibitor of 5-enolpyruvylshikimic acid 3-phosphate synthase. Biochem Biophys Res Commun 1980;94:1207–1212.
4. Kahan FM, Kahan JS, Cassidy PJ, Kropp H. The mechanism of action of fosfomycin (phosphonomycin). Ann NY Acad Sci 1974;235: 364–385.

5. Wanke C, Amrhein N. Evidence that the reaction of the UDP-*N*-acetylglucosamine 1-carboxyvinyltransferase proceeds through the *O*-phosphothioketal of pyruvic acid bound to Cys115. Eur J Biochem 1993;218:861–870.
6. Marquardt JL, Brown DE, Lane WS, Haley TM, Ichikawa Y, Wong C-H, Walsh CT. Kinetics, stoichiometry, and identification of the reactive thiolate in the inactivation of UDP-GlcNAc enolpyruvoyl transferase by the antibiotic fosfomycin. Biochemistry 1994;33: 10646–10651.
7. Schönbrunn E, Sack S, Eschenburg S, Perrakis A, Krekel F, Amrhein N, Mandelkow E. Crystal structure of UDP-*N*-acetylglucosamine enolpyruvyltransferase, the target of the antibiotic fosfomycin. Structure (London) 1996;4:1065–1075.
8. Schönbrunn E, Svergun DI, Amrhein N, Koch, MHJ. Studies on the conformational changes in the bacterial cell wall biosynthetic enzyme UDP-*N*-acetylglucosamine *enol*pyruvyltransferase (MurA). Eur J Biochem 1998;253:406–412.
9. Skarzynski T, Mistry A, Wonacott A, Hutchinson SE, Kelly VA, Duncan K. Structure of UDP-*N*-acetylglucosamine enolpyruvyl transferase, an enzyme essential for the synthesis of bacterial peptidoglycan, complexed with substrate UDP-*N*-acetylglucosamine and the drug fosfomycin. Structure (London) 1996;4: 1465–1474.
10. Skarzynski T, Kim DH, Lees WJ, Walsh CT, Duncan K. Stereochemical course of enzymatic enolpyruvyl transfer and catalytic conformation of the active site revealed by the crystal structure of the fluorinated analogue of the reaction tetrahedral intermediate bound to the active site of C115A mutant of MurA. Biochemistry 1998;37:2572–2577.
11. Schönbrunn E, Eschenburg S, Krekel F, Luger K, Amrhein N. The role of the loop containing residue 115 in the induced-fit mechanism of the bacterial cell wall biosynthetic enzyme MurA. Biochemistry 2000;39:2164–2173.
12. Wanke C, Falchetto R, Amrhein N. The UDP-*N*-acetylglucosamine 1-carboxyvinyl-transferase of *Enterobacter cloacae.* Molecular cloning, sequencing of the gene and overexpression of the enzyme. FEBS Lett 1992;301:271–276.
13. Sack S, Dauter Z, Wanke C, Amrhein N, Mandelkow E, Schönbrunn E. Crystallization and preliminary X-ray diffraction analysis of UDP-*N*-acetylglucosamine enolpyruvyltransferase of *Enterobacter cloacae*. J Struct Biol 1996;117:73–76.
14. Otwinowski, Z, Minor W. Processing of X-ray diffraction data collected in oscillation mode. Methods Enzymol 1997;276:307–326.
15. Brünger AT, Adams PD, Clore GM, DeLano WL, Gros P, Grosse-Kunstleve RW, Jiang JS, Kuszewski J, Nilges M, Pannu NS, Read RJ, Rice LM, Simonson T, Warren GL. Crystallography & NMR System (CNS): a new software system for macromolecular structure determination. Acta Cryst. 1998;D54:905–921.
16. Brünger AT. Free R value: A novel statistical quantity for assessing the accuracy of crystal structures. Nature 1992;335:472–475.
17. Jones TA, Zou J-Y, Cowan SW, Kjeldgaard M. Improved methods for building protein models in electron density maps and the location of errors in these models. Acta Cryst 1991;A47:110–119.
18. Read RJ. Improved Fourier coefficients for maps using phases from partial structures with errors. Acta Cryst. 1986;A42:140–149.
19. Ramakrishnan C, Ramachandran GN. Stereochemical criteria for polypeptide and protein chain conformations. II. Allowed conformations for a pair of peptide units. Biophys J 1965;5:909–933.
20. Laskowski RA, MacArthur MW, Moss DS, Thornton JM. PROCHECK: a program to check the stereochemical quality of protein structures. J Appl Cryst 1993;26:283–291.
21. Kabsch W, Sander C. Dictionary of protein secondary structure: pattern recognition of hydrogen-bonded and geometrical features. Biopolymers 1983;22:2577–2637.
22. Aswad DW, editor. Deamidation and isoaspartate formation in peptides and proteins. Boca Raton: CRC Press; 1994.
23. Noguchi S, Satow Y, Uchida T, Sasaki C, Matsuzaki T. Crystal structure of *ustilago spaerogena* ribonuclease U_2 at 1.8 Å resolution. Biochemistry 1995;34:15583–15591.
24. Capasso S, Di Donato A, Esposito L, Sica F, Sorrentino G, Vitagliano L, Zagari A, Mazzarella L. Deamidation in proteins: the crystal structure of bovine pancreatic ribonuclease with an isoaspartyl residue at position 67. J Mol Biol 1996;257:492–496.
25. Noguchi S, Miyawaki K, Satow Y. Succinimide and isoaspartate residues in the crystal structures of hen egg-white lysozyme complexed with tri-N-acetylchitotriose. J Mol Biol 1998;278:231–238.
26. Brennan TV, Clarke S. Deamidation and isoaspartate formation in model synthetic peptides: the effects of sequence and solution environment. In: Aswad DW, editor. Deamidation and isoaspartate formation in peptides and proteins. Boca Raton: CRC Press; 1994. p 66–89.
27. Geiger T, Clarke S. Deamidation, isomerization, and racemization at asparaginyl and aspartyl residues in peptides: succinimide-linked reactions that contribute to protein degradation. J Biol Chem 1987;262:785–794.
28. Wright, HT. Amino acid abundance and sequence data: clues to the biological significance of nonenzymatic asparagine and glutamine deamidation in proteins. In: Aswad DW, editor. Deamidation and isoaspartate formation in peptides and proteins. Boca Raton: CRC Press; 1994. p 230–251.
29. Wright HT. Nonenzymatic deamidation of asparaginyl and glutaminyl residues in proteins. Crit Rev Biochem Mol Biol 1991;26: 1–52.
30. Krekel F. Dissertation. ETH Zurich, Switzerland; 1998.
31. Aswad DW. Purification and properties of protein-L-isoaspartyl methyltransferase. In: Aswad DW, editor. Deamidation and isoaspartate formation in peptides and proteins. Boca Raton: CRC Press; 1994. p 32–45.
32. Fu JC, Ding L, Clarke S. Purification, gene cloning, and sequence analysis of an L-isoaspartyl protein carboxyl methyltransferase from *Escherichia coli*. J. Biol. Chem. 1991;22:14562–14572.
33. Nicholls A, Sharp KA, Honig B. Protein Folding and association: insights from the interfacial and thermodynamic properties of hydrocarbons. Proteins 1991;11:281–296.
34. Kraulis PJ. MOLSCRIPT: a program to produce both detailed and schematic plots of protein structures. J Appl Cryst 1991;24:946–950.
35. Esnouf RMJ. An extensively modified version of MolScript that includes greatly enhanced coloring capabilities. Mol Graphics 1997;15:132–134.